10202 *Inorg. Chem.* **2009**, *48*, 10202–10210
DOI: 10.1021/ic9011982

Inorganic Chemistry
Article

Luminescence Vapochromism of a Platinum(II) Complex for Detection of Low Molecular Weight Halohydrocarbon

Jun Ni,[†] Yu-Hui Wu,[†] Xu Zhang,[†] Bin Li,[†] Li-Yi Zhang,[†] and Zhong-Ning Chen*[,†,‡]

[†]*State Key Laboratory of Structural Chemistry, Fujian Institute of Research on the Structure of Matter, Chinese Academy of Sciences, Fuzhou, Fujian 350002, China, and* [‡]*State Key Laboratory of Organometallic Chemistry, Shanghai Institute of Organic Chemistry, Chinese Academy of Sciences, Shanghai 200032, China*

Received June 22, 2009

Platinum(II) complex [Pt($Me_3SiC{\equiv}CbpyC{\equiv}CSiMe_3$)($C{\equiv}CPh)_2$] (**1**) with 5,5-bis(trimethylsilylethynyl)-2,2′-bipyridine ($Me_3SiC{\equiv}CbpyC{\equiv}CSiMe_3$) and phenylacetylene ($PhC{\equiv}CH$) exhibits unusual luminescence vapochromism to volatile organic compounds (VOCs) including CH_2Cl_2, $CHCl_3$, and CH_3I, which is useful for detection of volatile halohydrocarbon with one carbon atom and molecular weight less of than 150. Crystal structural determination of **1**, **1**·$CHCl_3$, **1**·$^1/_2(CH_2ClCH_2Cl)$, and **1**·$^1/_2$(toluene) revealed a staggered packing for **1**·$CHCl_3$ whereas there was an antiparallel packing for other three structures in stacking of planar platinum(II) moieties. The Pt···Pt distance is 3.302(1) Å in **1**·$CHCl_3$, whereas it is >4.0 Å in the other three structures. Complex **1** displays bright orange luminescence in dichloromethane solution, arising from π(phenylacetylide)→$\pi^*(Me_3SiC{\equiv}CbpyC{\equiv}CSiMe_3)$ ^{3}LLCT and d(Pt)→$\pi^*(Me_3SiC{\equiv}CbpyC{\equiv}CSiMe_3)$ ^{3}MLCT triplet states which are supported by DFT calculation. The solid-state emission occurs at approximately 762 nm for **1**·VOC (VOC = CH_2Cl_2, $CHCl_3$, and CH_3I), whereas it was at approximately 562 (603sh) or 603 (562sh) nm for **1** and other **1**·VOC, corresponding to a vapochromic response shift of approximately 160−200 nm. The dramatic vapochromism and vapoluminescence of **1** to the vapor of CH_2Cl_2, $CHCl_3$, or CH_3I are induced by a reversible conversion of the emissive state from ^{3}MLCT/^{3}LLCT character to ^{3}MMLCT/^{3}LLCT state.

Introduction

Vapochromic and vapoluminescent materials have attracted increasing attention in view of their potential applications as chemosensors for detection of volatile organic compounds (VOCs) in the environment and the workplace.[1] They usually display reversible and naked eye perceivable color or luminescence changes upon exposure to specific VOCs,[1−28] resulting from a change in metal−metal contact or the appearance of weak interactions including hydrogen bonding, solvent−metal bonds, and aromatic $\pi-\pi$ stacking.

*To whom correspondence should be addressed. E-mail: czn@fjirsm.ac.cn.

(1) (a) Daws, C. A.; Exstrom, C. L.; Sowa, J. R., Jr.; Mann, K. R. *Chem. Mater*. **1997**, *9*, 363. (b) Buss, C. E.; Mann, K. R. *J. Am. Chem. Soc*. **2002**, *124*, 1031. (c) McGee, K. A.; Marquardt, B. J.; Mann, K. R. *Inorg. Chem*. **2008**, *47*, 9143. (d) Buss, C. E.; Anderson, C. E.; Pomije, M. K.; Lutz, C. M.; Britton, D.; Mann, K. R. *J. Am. Chem. Soc*. **1998**, *120*, 7783. (e) Exstrom, C. L.; Pomije, M. K.; Mann, K. R. *Chem. Mater*. **1998**, *10*, 942. (f) Drew, S. M.; Janzen, D. E.; Buss, C. E.; MacEwan, D. I.; Dublin, K. M.; Mann, K. R. *J. Am. Chem. Soc*. **2001**, *123*, 8414.

(2) (a) Albrecht, M.; Lutz, M.; Spek, A. L.; van Koten, G. *Nature* **2000**, *406*, 970. (b) Albrecht, M.; Gossage, R. A.; Lutz, M.; Spek, A. L.; van Koten, G. *Chem.—Eur. J*. **2000**, *6*, 1431.

(3) (a) Du, P. W.; Schneider, J.; Brennessel, W. W.; Eisenberg, R. *Inorg. Chem*. **2008**, *47*, 69. (b) Wadas, T. J.; Wang, Q.-M.; Kim, Y.-j.; Flaschenreim, C.; Blanton, T. N.; Eisenberg, R. *J. Am. Chem. Soc*. **2004**, *126*, 16841.

(4) Stork, J. R.; Olmstead, M. M.; Balch, A. L. *J. Am. Chem. Soc*. **2005**, *127*, 6512.

(5) (a) White-Morris, R. L.; Olmstead, M. M.; Jiang, F. L.; Tinti, D. S.; Balch, A. L. *J. Am. Chem. Soc*. **2002**, *124*, 2327. (b) Olmstead, M. M.; Jiang, F. L.; Attar, S.; Balch, A. L. *J. Am. Chem. Soc*. **2001**, *123*, 3260. (c) White-Morris, R. L.; Olmstead, M. M.; Balch, A. L. *J. Am. Chem. Soc*. **2003**, *125*, 1033.

(6) Mansour, M. A.; Connick, W. B.; Lachicotte, R. J.; Gysling, H. J.; Eisenberg, R. *J. Am. Chem. Soc*. **1998**, *120*, 1329.

(7) (a) Fernandez, E. J.; Lopez-de-Luzuriaga, J. M.; Monge, M.; Olmos, M. E.; Perez, J.; Laguna, A.; Mohamed, A. A.; Fackler, J. P., Jr. *J. Am. Chem. Soc*. **2003**, *125*, 2022. (b) Fernández, E. J.; López-de-Luzuriaga, J. M.; Monge, M.; Olmos, M. E.; Puelles, R. C.; Laguna, A.; Mohamed, A. A.; Fackler, J. P., Jr. *Inorg. Chem*. **2008**, *47*, 8069. (c) Fernandez, E. J.; Lopez-de-Luzuriaga, J. M.; Monge, M.; Montiel, M.; Olmos, M. E.; Perez, J.; Laguna, A.; Mendizabai, F.; Mohamed, A. A.; Fackler, J. P., Jr. *Inorg. Chem*. **2004**, *43*, 3573.

(8) (a) Kato, M.; Omura, A.; Toshikawa, A.; Kishi, S.; Sugimoto, Y. *Angew. Chem., Int. Ed*. **2002**, *41*, 3183. (b) Kato, M. *Bull. Chem. Soc. Jpn*. **2007**, *80*, 287.

(9) (a) Che, C. M.; Fu, W. F.; Lai, S. W.; Hou, Y. J.; Liu, Y. L. *Chem. Commun*. **2003**, 118. (b) Kui, S. C. F.; Chui, S. S. Y.; Che, C. M.; Zhu, N. *J. Am. Chem. Soc*. **2006**, *128*, 8297. (c) Lu, W.; Chan, M. C. W.; Zhu, N; Che, C. M.; He, Z.; Wong, K. Y. *Chem.—Eur. J*. **2003**, *9*, 6155. (d) Lu, W.; Chan, M. C. W.; Cheung, K.-K.; Che, C.-M. *Organometallics* **2001**, *20*, 2477.

(10) (a) Forniés, J.; Fuertes, S.; López, A.; Martín, J. A.; Sicilia, V. *Inorg. Chem*. **2008**, *47*, 7166. (b) Grzesiak, A. L.; Matzger, A. *Inorg. Chem*. **2007**, *46*, 453.

(11) Muro, M. L.; Daws, C. A.; Castellano, F, N. *Chem. Commun*. **2008**, 6134.

(12) (a) Grove, L. J.; Oliver, A. G.; Krause, J. A.; Connick, W. B. *Inorg. Chem*. **2008**, *47*, 1408. (b) Grove, L. J.; Rennekamp, J. M.; Jude, H.; Connick, W. B. *J. Am. Chem. Soc*. **2004**, *126*, 1594.

Published on Web 09/25/2009

A range of transition metal complexes including those of platinum(II),[1−4,8−17] gold(I),[5−7,25] zinc(II),[18−20] iridium(III),[24] copper(I),[21,22] copper(II),[23] ruthenium(II),[26] palladium(II),[1d,17] and so forth have been found to exhibit intriguing vapochromism to specific VOCs.

Square-planar platinum(II) complexes that stack in the solid states frequently exhibit Pt−Pt interactions that significantly lower the metal-to-ligand charge transfer (MLCT) energy.[29,30] More interestingly, the solid-state stacked structures can be perturbed by interactions with interstitial solvent molecules. Incorporation of the organic vapor into the solid phase can significantly modify the stacking patterns of square-planar platinum(II) complexes in crystal lattices and consequently the Pt−Pt contacts by filling some of the free volume with the VOCs, thus inducing dramatic changes in color and emission that are perceptible to the human eye and even deeper under UV irradiation.[1−4,8−17] Unusual luminescence vapochromism of a bis(σ-acetylide) platinum(II) complex with 5,5′-bis(trimethylsilylethynyl)-2,2′-bipyridine ($Me_3SiC{\equiv}CbpyC{\equiv}CSiMe_3$) and 5-ethynyl-2,2′-bipyridine ($HC{\equiv}Cbpy$) has been recently described by us.[31] This complex exhibits highly selective and reversible color and luminescence changes to a variety of VOCs with the emission shift from 562 to 747 nm, corresponding to a vapochromic response shift of 185 nm.

We report herein the syntheses, crystal structures, and vapochromic and vapoluminescent properties of a new bis(σ-acetylide) platinum(II) complex (**1**) with $Me_3SiC{\equiv}CbpyC{\equiv}CSiMe_3$ and $HC{\equiv}CPh$ (phenylacetylene). This complex shows selective and reversible color and luminescence responses to organic vapors including CH_2Cl_2, $CHCl_3$, and CH_3I, which is useful for detection of halohydrocarbon with low molecular weight less than 150. Systematic studies on the crystal structures of **1** and **1**·VOC (VOC = chloroform, 1,2-dichloroethane, and toluene) have revealed unambiguously that the stacking patterns of planar platinum(II) moieties affect significantly the Pt···Pt distances and consequently the luminescence properties in the solid states.

Experimental Section

General Procedures and Materials. All operations were carried out under a dry argon atmosphere using Schlenk techniques and vacuum-line systems unless otherwise specified. The solvents were dried, distilled, and degassed prior to use except that those for spectroscopic measurements were of spectroscopic grade. 5,5′-Bis(trimethylsilylethynyl)-2,2′-bipyridine ($Me_3SiC{\equiv}CbpyC{\equiv}CSiMe_3$) was prepared by synthetic procedures described in literature.[32] Other reagents were purchased from commercial sources and used as received unless stated otherwise.

$Pt(Me_3SiC{\equiv}CbpyC{\equiv}CSiMe_3)Cl_2$. 5,5′-Bis(trimethylsilylethynyl)-2,2′-bipyridine (34.8 mg, 0.1 mmol) and $Pt(DMSO)_2Cl_2$ (42.2 mg, 0.1 mmol) were added to 50 mL of acetonitrile with stirring for 5 h at ambient temperature. The product was purified by chromatography on a silica gel column using dichloromethane−methanol (v/v = 50:1) as eluent and isolated as a yellow solid. Yield: 78%. Anal. Calcd for $C_{20}H_{24}Cl_2N_2PtSi_2$: C, 39.09; H, 3.94; N, 4.56%. Found: C, 38.99; H, 4.03; N, 4.47%. ^{1}H NMR ($CDCl_3$, ppm): 0.31 (s, 18H, CH_3), 7.87 (d, 2H, J = 5 Hz, bpy), 8.15 (d, 2H, J = 5 Hz, bpy), 9.86 (s, 2H, bpy). IR (KBr disk, cm^{-1}): 2168m (C≡C), 1258m (Si−C).

$Pt(Me_3SiC{\equiv}CbpyC{\equiv}CSiMe_3)(PhC{\equiv}C)_2$ (1). $Pt(Me_3SiC{\equiv}CbpyC{\equiv}CSiMe_3)Cl_2$ (122 mg, 0.20 mmol), phenylacetylene (51 mg, 0.50 mmol), CuI (1 mg), and diisopropylamine (2 mL) were added to 50 mL of dichloromethane with stirring for 1 d at ambient temperature. The product was purified by chromatography on a silica gel column using dichloromethane−methanol (v/v = 75:1) as eluent. Yield: 76%. Anal. Calcd for $C_{36}H_{34}N_2PtSi_2$: C, 57.97; H, 4.59; N, 3.76. Found: C, 57.88; H, 4.61; N, 3.72. ESI-MS (m/z): 747 $[M + H]^+$. ^{1}H NMR (d_6-DMSO, ppm): 0.28 (s, 18H, CH_3), 7.23(t, 2H, J = 7 Hz, C_6H_5), 7.31 (t, 4H, J = 7.4 Hz, C_6H_5), 7.35 (d, 4H, J = 7.3 Hz, C_6H_5), 8.50 (d, 2H, J = 8.4 Hz, bpy), 8.70 (d, 2H, J = 8.4 Hz, bpy), 9.67 (s, 2H, bpy). IR (KBr disk, cm^{-1}): 2114s (C≡CPt); 2163m ($C{\equiv}CSiMe_3$), 1248m (Si−C).

Physical Measurements. UV−vis absorption spectra were measured on a Perkin-Elmer Lambda 25 UV−vis spectrophotometer. Infrared spectra (IR) were recorded on a Magna 750 FT-IR spectrophotometer with KBr pellets. Elemental analyses (C, H, N) were carried out on a Perkin-Elmer model 240 C elemental analyzer. Electrospray mass spectrometry (ES-MS) were performed on a Finnigan LCQ mass spectrometer using dichloromethane methanol mixtures as mobile phases. Emission and excitation spectra were recorded on a Perkin-Elmer LS55 luminescence spectrometer with a red-sensitive photomultiplier type R928. Emission lifetimes in solid states and degassed solutions were determined on an Edinburgh analytical instrument (F900 fluorescence spectrometer) using an LED laser at 440 nm excitation. The emission quantum yield (Φ_{em}) of **1** in degassed dichloromethane solution at room temperature was calculated by $\Phi_s = \Phi_r(B_r/B_s)(n_s/n_r)^2(D_s/D_r)$ using $[Ru(bpy)_3](PF_6)_2$ in acetonitrile as the standard (Φ_{em} = 0.062), where the subscripts r and s denote reference standard and the sample solution, respectively, and n, D, and Φ are the refractive index of

(13) Yam, V. W. W.; Wong, K. M. C.; Zhu, N. *J. Am. Chem. Soc.* **2002**, *124*, 6506.
(14) Pattacini, R.; Giansante, C; Ceroni, P.; Maestri, M.; Braunstein, P. *Chem.—Eur. J.* **2007**, *13*, 10117.
(15) Iguchi, H.; Iguchi, S.; Takaishi, S.; Kajiwara, T.; Miyasaka, H.; Yamashita, M.; Matsuzaki, H.; Okamoto, H. *J. Inorg. Org. Polym. Mater.* **2009**, *19*, 85.
(16) Yamashita, M.; Takizawa, K.; Matsunaga, S.; Kawakami, D.; Iguchi, H.; Takaishi, S.; Kajiwara, T.; Iwahori, F.; Ishii, T.; Miyasaka, H.; Sugiura, K.; Matsuzaki, H.; Kishida, H.; Okamoto, H. *Bull. Chem. Soc. Jpn.* **2006**, *79*, 1404.
(17) Sluch, I. M.; Miranda, A. J.; Slaughter, L. M. *Cryst. Growth Des.* **2009**, *9*, 1267.
(18) Pang, J.; Marcotte, E. J. P; Seward, C.; Brown, R. S.; Wang, S. *Angew. Chem., Int. Ed.* **2001**, *40*, 4042.
(19) Das, S.; Bharadwaj, P. K. *Inorg. Chem.* **2006**, *45*, 5257.
(20) Mizukami, S.; Houjou, H.; Sugaya, K.; Koyama, E.; Tokuhisa, H.; Sasaki, T.; Kanesato, M. *Chem. Mater.* **2005**, *17*, 50.
(21) Cariati, E.; Bu, X.; Ford, P. C. *Chem. Mater.* **2000**, *12*, 3385.
(22) Dias, H. V. R.; Diyabalanage, H. V. K.; Omary, M. A. R.; Franzman, M. A.; Omary, M. A. *J. Am. Chem. Soc.* **2003**, *125*, 12072.
(23) (a) Lefebvre, J.; Batchelor, R. J.; Leznoff, D. B. *J. Am. Chem. Soc.* **2004**, *126*, 16117. (b) Katz, M. J.; Ramnial, T.; Yu, H.-Z.; Leznoff, D. B. *J. Am. Chem. Soc.* **2008**, *130*, 10662.
(24) Liu, Z. W.; Bian, Z. Q.; Bian, J.; Li, Z. D.; Nie, D. B.; Huang, C. H. *Inorg. Chem.* **2008**, *47*, 8025.
(25) (a) Luquin, A.; Bariain, C.; Vergara, E.; Cerrada, E.; Garrido, J.; Matias, I. R.; Laguna, M. *Appl. Organomet. Chem.* **2005**, *19*, 1232. (b) Luquin, A.; Elosua, C.; Vergara, E.; Estella, J.; Cerrada, E.; Bariain, C.; Matias, I. R.; Garrido, J.; Laguna, M. *Gold Bull.* **2007**, *40*, 225.
(26) Abe, T.; Shinozaki, K. *Inorg. Chem.* **2005**, *44*, 849.
(27) Bailey, R. C.; Hupp, J. T. *J. Am. Chem. Soc.* **2002**, *124*, 6767.
(28) Beauvais, L. G.; Shores, M. P.; Long, J. R. *J. Am. Chem. Soc.* **2000**, *122*, 2763.
(29) (a) Miskowski, V. M.; Houlding, V. H. *Inorg. Chem.* **1991**, *30*, 4446. (b) Miskowski, V.; Houlding, V. H.; Che, C.-M.; Wang, Y. *Inorg. Chem.* **1993**, *32*, 2518.
(30) (a) Bailey, J. A.; Hill, M. G.; Marsh, R. E.; Miskowski, V. M.; Schaefer, W. P.; Gray, H. B. *Inorg. Chem.* **1995**, *34*, 4591. (b) Connick, W. B.; Henling, L. M.; Marsh, R. E.; Gray, H. B. *Inorg. Chem.* **1996**, *35*, 6261.
(31) Ni, J.; Zhnag, L.-Y.; Wen, H.-M.; Chen, Z.-N. *Chem. Commun.* **2009**, 3801.
(32) Grosshenny, V.; Romero, F. M.; Ziessel, R. *J. Org. Chem.* **1997**, *62*, 1491.

Table 1. Crystallographic Data for **1**, **1**·$CHCl_3$, **1**·$^1/_2CH_2ClCH_2Cl$, and **1**·$^1/_2$Toluene

	1	**1**·$CHCl_3$	**1**·$^1/_2CH_2ClCH_2Cl$	**1**·$^1/_2$toluene
empirical formula	$C_{36}H_{34}N_2PtSi_2$	$C_{37}H_{35}Cl_3N_2PtSi_2$	$C_{37}H_{36}ClN_2PtSi_2$	$C_{39.5}H_{38}N_2PtSi_2$
formula weight	745.92	865.29	795.40	791.99
space group	$P\bar{1}$	$C2/c$	$P\bar{1}$	$I4_1/a$
a, Å	10.367(10)	26.946(9)	7.138(2)	28.228(1)
b, Å	12.103(12)	18.617(6)	13.892(3)	28.228(1)
c, Å	14.724(15)	15.064(5)	19.167(5)	20.154(1)
α, deg	67.09(3)		106.88(1)	
β, deg	78.16(4)	91.37(1)	93.42(1)	
γ, deg	82.13(5)		97.37(1)	
V, Å^3	1662(3)	7555(4)	1794.5(8)	16058.6(6)
Z	2	8	2	16
ρ_{calcd}, g/cm^{-3}	1.490	1.522	1.472	1.310
μ, mm^{-1}	4.319	4.018	4.078	3.581
radiation (λ, Å)	0.71073	0.71073	0.71073	0.71073
temp (K)	298	298	298	298
R1(F_o)[a]	0.0864	0.0487	0.0434	0.0460
wR2(F_o^2)[b]	0.2312	0.0802	0.1061	0.1411
GOF	1.038	1.069	1.116	1.182

[a] $R1 = \sum|F_o - F_c|/\sum F_o$. [b] $wR2 = \sum[w(F_o^2 - F_c^2)^2]/\sum[w(F_o^2)]^{1/2}$.

the solvents, the integrated intensity, and the luminscence quantum yield, respectively. The quantity B is calculated by $B = 1 - 10^{-AL}$, where A is the absorbance at the excitation wavelength and L is the optical path length. The vapor absorbing was operated at room temperature under a dinitrogen atmosphere.

Crystal Structural Determination. Crystals of **1** were grown by diffusion of hexane into the dichloromethane solution, whereas those of **1**·$CHCl_3$, **1**·$^1/_2(CH_2ClCH_2Cl)$, and **1**·$^1/_2$(toluene) were obtained by layering petroleum ether onto the corresponding chloroform, 1,2-dichloroethane, and toluene solutions of **1**, respectively. Data collection was performed on Mercury CCD diffractometer by the ω scan technique at room temperature using graphite-monochromated Mo Kα (λ = 0.71073 Å) radiation. The CrystalClear software package was used for data reduction and empirical absorption correction. The structures were solved by direct methods. The heavy atoms were located from E-map, and the rest of the non-hydrogen atoms were found in subsequent Fourier maps. All non-hydrogen atoms were refined anisotropically, while the hydrogen atoms were generated geometrically and refined with isotropic thermal parameters. The structures were refined on F^2 by full-matrix least-squares methods using the SHELXTL−97 program package.[33] The crystallographic data are summarized in Table 1.

Theoretical Methodology. The computational method used was density functional theory (DFT)[34] with the gradient corrected correlation functional PBE1PBE.[35] Since the PBE1PBE gave the best results in terms of structural parameters and simulation of UV−vis properties by comparing different functionals (Supporting Information), the geometry structure of [Pt($Me_3SiC{\equiv}Cbpy$-$C{\equiv}CSiMe_3$)($C{\equiv}CPh)_2$] (**1**) was optimized as an isolated molecule from the solvent phase at the DFT level. We performed geometry optimization from initial geometry of C_1 symmetry at first and confirmed that the stable geometry of **1** was C_2 symmetry in the ground state. The stable geometry of the C_2 symmetry was thus recalculated. On the basis of the structure, 40 singlet and 6 triplet excited states were obtained to determine the vertical excitation energies for **1** in dichloromethane using the time-dependent DFT (TD-DFT) calculations.[36,37] The polarized continuum model method (PCM)[38] with dichloromethane as solvent was used to calculate all the electronic structures in solution. To compare the different transition characters that contribute to the absorption and emission spectra of **1**·VOC in the solid states, two types of crystal structures including **1**·$CHCl_3$ and **1**·$^1/_2CH_2ClCH_2Cl$ were used for calculations. **1**·$CHCl_3$ displays a discrete staggered stacking in the crystal packing with Pt···Pt distance of approximately 3.3 Å to form a ligand-unsupported dimeric structure so that the calculations based on this platinum(III) dimer correspond to the behavior of **1**·$CHCl_3$ in the crystalline state. In contrast, **1**·$^1/_2CH_2ClCH_2Cl$ exhibits an antiparallel packing in stacking of planar platinum(II) moieties with the shortest Pt···Pt distance of approximately 4.4 Å. On the basis of the two different crystal structures, 60 singlet and 6 triplet excited states for **1**·$CHCl_3$ and **1**·$^1/_2CH_2ClCH_2Cl$ were obtained using the time-dependent DFT calculations, respectively. In these calculations, the SDD[39] basis set consisting of effective core potentials (ECPs) for the platinum(II) atom and 6-31G(p,d) basis set for the remaining atoms were used. To precisely describe the molecular properties, one additional f-type polarization function was implemented for platinum(II) atom (α = 0.18),[40] and the 6-31G(p,d) basis set was used for the remaining atoms. All the calculations were performed using the Gaussian 03 program package.[41]

(33) Sheldrick, G. M. *SHELXL-97, Program for the Refinement of Crystal Structures*; University of Göttingen: Göttingen, Germany, 1997.
(34) Runge, E.; Gross, E. K. U. *Phys. Rev. Lett.* **1984**, *52*, 997.
(35) Perdew, J. P.; Burke, K.; Ernzerhof, M. *Phys. Rev. Lett.* **1997**, *78*, 1396.
(36) Casida, M. E.; Jamorski, C.; Casida, K. C.; Salahub, D. R. *J. Chem. Phys.* **1998**, *108*, 4439.
(37) Stratmann, R. E.; Scuseria, G. E.; Frisch, M. J. *J. Chem. Phys.* **1998**, *109*, 8218.
(38) (a) Cossi, M.; Scalmani, G.; Regar, N.; Barone, V. *J. Chem. Phys.* **2002**, *117*, 43. (b) Barone, V.; Cossi, M. *J. Chem. Phys.* **1997**, *107*, 3210.
(39) Schwerdtfeger, P.; Dolg, M.; Schwarz, W. H. E.; Bowmaker, G. A.; Boyd, P. D. W. *J. Chem. Phys.* **1989**, *91*, 1762.
(40) (a) Pyykkö, P.; Runeberg, N.; Mendizabal, F. *Chem.—Eur. J.* **1997**, *3*, 1451. (b) Pyykkö, P.; Mendizabal, F. *Chem.—Eur. J.* **1997**, *3*, 1458.
(41) Frisch, M. J.; Trucks, G. W.; Schlegel, H. B.; Scuseria, G. E.; Robb, M. A.; Cheeseman, J. R.; Montgomery, J. A., Jr.; Vreven, T.; Kudin, K. N.; Burant, J. C.; Millam, J. M.; Iyengar, S. S.; Tomasi, J.; Barone, V.; Mennucci, B.; Cossi, M.; Scalmani, G.; Rega, N.; Petersson, G. A.; Nakatsuji, H.; Hada, M.; Ehara, M.; Toyota, K.; Fukuda, R.; Hasegawa, J.; Ishida, M.; Nakajima, T.; Honda, Y.; Kitao, O.; Nakai, H.; Klene, M.; Li, X.; Knox, J. E.; Hratchian, H. P.; Cross, J. B.; Bakken, V.; Adamo, C.; Jaramillo, J.; Gomperts, R.; Stratmann, R. E.; Yazyev, O.; Austin, A. J.; Cammi, R.; Pomelli, C.; Ochterski, J. W.; Ayala, P. Y.; Morokuma, K.; Voth, G. A.; Salvador, P.; Dannenberg, J. J.; Zakrzewski, V. G.; Dapprich, S.; Daniels, A. D.; Strain, M. C.; Farkas, O.; Malick, D. K.; Rabuck, A. D.; Raghavachari, K.; Foresman, J. B.; Ortiz, J. V.; Cui, Q.; Baboul, A. G.; Clifford, S.; Cioslowski, J.; Stefanov, B. B.; Liu, G.; Liashenko, A.; Piskorz, P.; Komaromi, I.; Martin, R. L.; Fox, D. J.; Keith, T.; Al-Laham, M. A.; Peng, C. Y.; Nanayakkara, A.; Challacombe, M.; Gill, P. M. W.; Johnson, B.; Chen, W.; Wong, M. W.; Gonzalez, C.; Pople, J. A. *Gaussian 03*, Revision C.02; Gaussian, Inc.: Wallingford, CT, 2004.

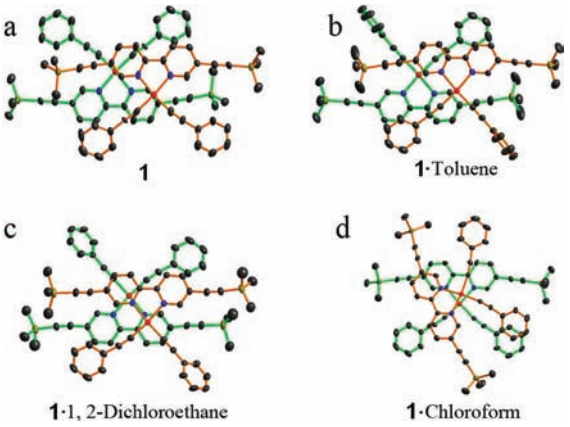

Figure 1. Stacking patterns of adjacent planar platinum(II) moieties. (a) **1**, (b) **1**·toluene, (c) **1**·$^1/_2CH_2ClCH_2Cl$, and (d) **1**·$CHCl_3$, showing a staggered packing for **1**·$CHCl_3$ and an antiparallel packing for the other three structures.

Results and Discussion

Preparation and Characterization. Complex **1** was prepared by reaction of the precursor Pt($Me_3SiC{\equiv}$ CbpyC${\equiv}$C$SiMe_3$)Cl_2 with phenylacetylene in dichloromethane solution in the presence of CuI and $^iPr_2NH$. The solid-state **1**·VOCs were obtained through recrystallization in the corresponding solutions by layering petroleum ether. **1** was characterized by elemental analyses, ESI-MS spectrometry, and ^{1}H NMR and IR spectroscopy. The crystal structures of **1**, **1**·$CHCl_3$, **1**·$^1/_2(CH_2ClCH_2Cl)$, and **1**·$^1/_2$(toluene) were determined by X-ray crystallography. The solvate VOC in **1**·VOC was well-defined through IR and ^{1}H NMR spectroscopy and thermal analysis−mass spectrometry in addition to crystal structural determination. The proton signals of solvate VOCs were all observed in the ^{1}H NMR spectra of **1**·VOC with various solvate VOCs. The solvate VOC in **1**·VOC are lost at 50−160 °C and distinctly detected by thermal analysis−mass spectrometry (Figures S1−S8, Supporting Information), demonstrating that VOCs are indeed inserted into the crystal lattices of planar platinum(II) structures.

Stacking patterns of adjacent planar platinum(II) moieties for **1**, **1**·$^1/_2(CH_2ClCH_2Cl)$, **1**·$^1/_2$(toluene), and **1**·$CHCl_3$ are depicted in Figure 1. Selected interatomic distances and bonding angles of **1**, **1**·$CHCl_3$, **1**·$^1/_2$-(CH_2ClCH_2Cl), and **1**·$^1/_2$(toluene) are summarized in Table 2. The square-planar platinum(II) moieties adopt two different types of stacking patterns in the crystal packing. The adjacent platinum(II) moieties display an antiparallel stacking pattern in **1** (Figure 1a), **1**·$^1/_2$-(toluene) (Figure 1b), and **1**·$^1/_2(CH_2ClCH_2Cl)$ (Figure 1c) so as to induce a severe slide from one another.[31] The shortest Pt···Pt separation is 5.042(5) Å for **1**, 4.409(1) Å for **1**·$^1/_2(CH_2ClCH_2Cl)$, and 4.727(1) Å for **1**·$^1/_2$(toluene) so that there are no metallophilic interactions. In contrast, the crystal packing in **1**·$CHCl_3$ (Figure 1d) exhibits a staggered pattern so that planar platinum(II) moieties are arranged in close proximity, giving a short Pt···Pt distance [3.302(1) Å] to form a dimeric structure through ligand-unsupported Pt−Pt contact. The dihedral angles between the least-squares planes of 2,2′-bipyridyl and phenylacetylide are 18.9 and 26.8° for **1**, 5.5 and 55.5° for **1**·$^1/_2(CH_2ClCH_2Cl)$, 11.7 and 75.8° for **1**·$^1/_2$(toluene), and 6.7 and 8.7° for **1**·$CHCl_3$. It appears that the better coplanarity between 2,2′-bipyridyl and phenylacetylide in **1**·$CHCl_3$ favors a staggered pattern in stacking of the planar platinum(II) moieties. Consequently, the stacking structures of planar platinum(II) moieties and Pt···Pt distances are significantly influenced by the solvate VOC molecules inserted in the crystal lattices.

Table 2. Selected Atomic Distances and Angles of **1** and **1**·VOC (VOC = $CHCl_3$, Toluene, and 1,2-Dichloroethane)

	1	**1**·$CHCl_3$	**1**·$^1/_2CH_2ClCH_2Cl$	**1**·$^1/_2$toluene
Pt···Pt	5.042(5)	3.302(1)	4.409(1)	4.727(1)
Pt1−N	2.068(11)	2.065(5)	2.068(5)	2.066(4)
	2.081(10)	2.069(5)	2.068(5)	2.077(4)
Pt1−C	1.928(10)	1.952(7)	1.957(6)	1.948(6)
	1.943(8)	1.951(6)	1.957(7)	1.969(5)
N−Pt1−N	78.1(4)	79.2(2)	78.8(2)	78.9(2)
C−Pt1−N	94.5(5)	94.7(2)	93.8(2)	97.1(2)
C−Pt1−N	95.3(5)	93.5(2)	96.9(2)	94.8(2)
C−Pt1−C	92.1(6)	92.6(2)	90.5(3)	89.2(2)
dihedral angle[a]	18.9	6.7	5.5	11.7
	26.8	8.7	55.5	75.8
dihedral angle[b]	45.6	15.0	51.4	75.1

[a] The dihedral angle between benzene ring and Pt coordination plane. [b] The dihedral angle between two benzene ring.

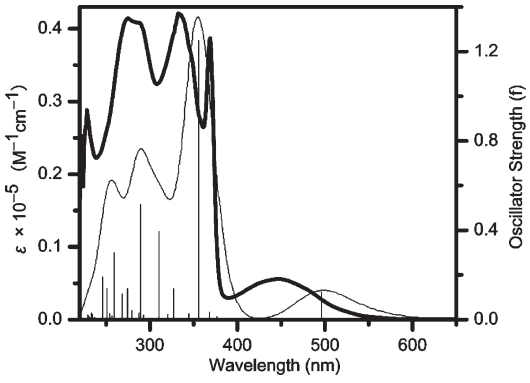

Figure 2. Calculated absorption spectrum (thin) with the TD-DFT method simulated by GaussSum 2.0 and measured UV−vis absorption spectrum (thick) of **1** in dichloromethane solution.

The solvate molecules are incorporated to the bis(σ-acetylide)platinum(II) structures through weak intermolecular interactions including hydrogen bonding and π−π stacking (Figure S9, Supporting Information). In crystal packing of **1**·$^1/_2(CH_2ClCH_2Cl)$, the solvate 1,2-dichloroethane molecules are connected to 2,2′-bipyridyl of the host structure by formation of the C−H···Cl hydrogen bond ($d_{Cl\cdots H}$ = 2.94(1) Å, $\theta_{C-H\cdots Cl}$ = 147.6 (2)°). For **1**·$CHCl_3$, there exists a substantial $Cl_3C-H\cdots\pi$ (C≡C) interaction ($d_{C\cdots H}$ = 2.56(1) Å, $\theta_{C-H\cdots C}$ = 147.9(2)°; $d_{C\cdots H}$ = 2.72(1) Å, $\theta_{C-H\cdots C}$ = 143.6 (1)°) between the solvate $CHCl_3$ molecule and ethynyl of the phenylacetylene. For **1**·$^1/_2$(toluene), there is a face-to-face arrangement between solvate toluene and pyridyl rings of 5,5′-bis(trimethylsilylethynyl)-2,2′-bipyridine with the central toluene···pyridyl distance being approximately 3.7 Å, suggesting that a weak aromatic π−π interaction is likely operating.

Photophysical Properties. The electronic absorption bands (Figure 2) of **1** in the UV region with extinction

Table 3. Absorption and Emission Data of **1** from MLCT/LLCT States in Various Solvents at 298 K

solvent	benzene	CH_2Cl_2	acetone	DMF	CH_3CN	MeOH
λ_{abs} [nm]	480	446	442	441	441	422
λ_{em} [nm]	631	616	624	615	618	619

coefficients (ε) on the order of 10^4 M^{-1} cm^{-1} are dominated by intraligand transitions (^{1}IL) in dichloromethane solution. The middle energy band centered at 348 and 368 nm are attributed to the admixture of $\pi\rightarrow\pi^*$(diimine) ^{1}IL, π(C≡CPh)$\rightarrow\pi^*$(diimine) ^{1}LLCT, and d(Pt)$\rightarrow\pi^*$(diimine) ^{1}MLCT states as supported from DFT calculations (vide infra). The low-energy broad absorption centered on 455 nm tailing to approximately 550 nm arises most likely from an admixture of d(Pt)$\rightarrow\pi^*$(diimine) ^{1}MLCT and π(C≡CPh)$\rightarrow\pi^*$(diimine) ^{1}LLCT transitions. As indicated in Table 3, this low-energy absorption maximum exhibits a blue shift in the order 480 nm (benzene) > 446 (CH_2Cl_2) > 422 nm (methanol) depending on the solvent polarity (Figure S10, Supporting Information), which is typical of MLCT/LLCT states.[42]

Upon irradiation of complex **1** at 350 nm < λ_{ex} < 550 nm, a bright orange luminescence was observed in both fluid solution and solid state at ambient temperature. With excitation at λ_{ex} > 350 nm, complex **1** displays a broad emission band at 616 nm with the lifetime of 0.13 μs and the quantum yield of 1.5% in degassed fluid dichloromethane at 298 K. The emission is somewhat solvent-dependent as indicated in Table 3, in which the emission wavelengths show small shifts in different solvents (Figure S10, Supporting Information). With increase of the solution concentrations, the emission energy shows some red-shift (Figure S11, Supporting Information).

Crystalline state **1** displays bright orange luminescence (Figure 3) at 561 and 603 nm with the lifetime of 2.12 μs at 298 K, resulting most likely from an admixture of ^{3}MLCT and ^{3}LLCT triplet states as supported from the DFT studies (vide infra). Vibronic-structured emission bands with vibrational progressional spacing of 1240 cm^{-1} (Figure S12, Supporting Information) are typical for the virational frequency of 2,2′-bipyridyl, suggesting the involvement of $Me_3SiC{\equiv}CbpyC{\equiv}CSiMe_3$ in the emissive states.[7a] Similarly, crystalline state **1**·$^1/_2$(CH_2ClCH_2Cl) and **1**·$^1/_2$(toluene) exhibit bright orange luminescence under UV light irradiation with two structured emission bands at approximately 563 and 605 nm, implying the same emission origin as that of crystalline state **1**. In contrast, crystalline state **1**·$CHCl_3$ is weakly luminescent (Figure 3) with a broad structureless emission band at approximately 760 nm. A dramatic red shift of the emission from **1** to **1**·$CHCl_3$ corresponds to a vapochromatic response shift of 160−200 nm, suggesting there has some difference between the emissive state of crystalline state **1** and that of **1**·$CHCl_3$. In view of the short Pt···Pt [3.302(1) Å] distance and substantial Pt−Pt contact in **1**·$CHCl_3$, the emissive origin is most likely ^{3}MMLCT/^{3}LLCT triplet state with a smaller HOMO−LUMO energy gap than

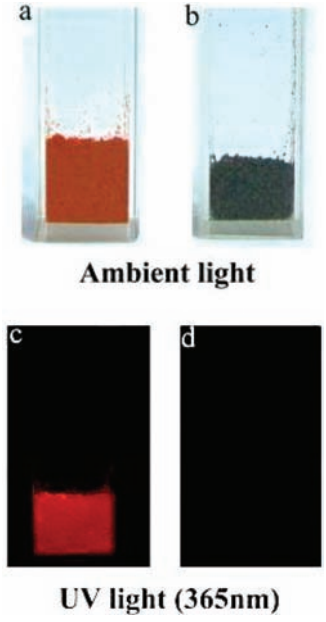

Figure 3. Photographic images of crystalline-state samples (a) **1** and (b) **1**·CH_2Cl_2 under ambient light, and (c) **1** and (d) **1**·CH_2Cl_2 under UV light irradiation (365 nm).

that of the corresponding ^{3}MLCT/^{3}LLCT state as supported by TD-DFT calculation (vide infra).

DFT Calculations. To elucidate the absorption and emission characters of **1** in dichloromethane, 40 singlet and 6 triplet excited states for **1** were calculated at the PBE1PBE/SDD (6-31G(d,p)) level with time-dependent DFT (TD-DFT) employing the ground state optimized geometry. The relative compositions of different energy levels in terms of composing fragments are presented in Table 4. As indicated in Table 4, the HOMO (highest occupied molecular orbital) is a π orbital localized predominantly on phenylacetylide (72%) with additional contribution from Pt(5d) (26%). The HOMO-1 is primarily resident on Pt(5d) (39.8%) and phenylacetylide (55.8%). The HOMO-3 consist of the compositions of 46.7% from phenylacetylide and 48.4% from Pt(5d). The HOMO-5, however, is mainly contributed by Pt(5d) (95.1%). The LUMO (lowest unoccupied molecular orbital) is mainly localized on $\pi^*(Me_3SiC{\equiv}CbpyC{\equiv}CSiMe_3)$ with a notable contribution from the central fused aromatic ring. The LUMO+1 and LUMO+2 are similarly centered on 2,2′-bipyridyl ligand, while the LUMO+4 and LUMO+5 are mainly contributed by the π^* orbital of phenylacetylide.

The main 40 singlet and 2 triplet vertical excitation energies of complex **1** (Table 5) from TD-DFT calculation agree well with the experimental values. Figure 2 shows the calculated absorption spectrum (bars) and the measured UV−vis spectrum of **1** in dichloromethane. The single electron density diagrams of the frontier molecular orbitals involved in the absorption are depicted in Figure 4. As shown in Table 5, the calculated lowest singlets at 556 nm (HOMO→LUMO) and 497 nm (HOMO-1→LUMO) can be assigned as ^{1}LLCT (ligand-to-ligand charge transfer) character mixed with some ^{1}MLCT (metal-to-ligand charge transfer) state. The intense excitation at approximately 355 nm arises mainly from HOMO-5→LUMO (76% contribution) and HOMO→LUMO+1

(42) Chan, S. C.; Chan, M. C. W.; Wang, Y.; Che, C. M.; Cheung, K. K.; Zhu, N. Y. *Chem.—Eur. J.* **2001**, *7*, 4180. (b) Hissler, M.; Connick, W. B.; Geiger, D. K.; McGarrah, J. E.; Lipa, D.; Lachicotte, R. J.; Eisengerg, R. *Inorg. Chem.* **2000**, *39*, 447.

Table 4. Partial Molecular Orbital Compositions (%) in the Ground State for **1** in Dichloromethane under the TD-DFT Calculations

		MO contribution (%)		
orbital	energy (eV)	Pt	$Me_3SiC{\equiv}CbpyC{\equiv}CSiMe_3$	$C{\equiv}CPh$
LUMO+5	−0.2547	3.2	7.0	89.8
LUMO+4	−0.5910	12.8	13.2	74.0
LUMO+2	−1.2253	1.0	97.0	2.0
LUMO+1	−1.5745	3.8	92.2	4.0
LUMO	−2.7832	5.6	92.5	1.9
HOMO	−5.6872	26.0	2.0	72.0
HOMO-1	−5.9144	39.8	4.4	55.8
HOMO-3	−6.7988	48.4	4.9	46.7
HOMO-5	−6.8478	95.1	3.2	1.8

(20% contribution) transitions, supporting a ^{1}MLCT state mixed with some ^{1}LLCT character. The absorption at 310 nm originates from HOMO-1→LUMO+2, suggesting a ^{1}LLCT transition mixed with some ^{1}MLCT character. The high-energy absorptions at $\lambda_{abs} < 300$ nm from HOMO→LUMO+4, HOMO-5→LUMO+2, and HOMO→LUMO+5 are mainly assigned as ^{1}IL (intraligand) transitions.

The HOMO→LUMO transitions from the lowest triplet excited states (T1) at 596 nm is in reasonable agreement with the experimentally measured emission (λ_{em} = 616 nm) in fluid dichloromethane, which is typical of ^{3}LLCT $^3[\pi(C{\equiv}CPh){\rightarrow}\pi^*(Me_3SiC{\equiv}CbpyC{\equiv}CSiMe_3)]$ and ^{3}MLCT $^3[5d(Pt){\rightarrow}\pi^*(Me_3SiC{\equiv}CbpyC{\equiv}CSiMe_3)]$ characters. Similarly, the T2 triplet excited state at 538 nm results from HOMO-1→LUMO transition ascribable also to ^{3}LLCT/^{3}MLCT character. It is noteworthy that the emission origins coincide well with the low-energy absorption characters mentioned above.

To further explore the nature of absorption and emission transitions of **1**·VOC in the solid states, TD-DFT calculations were preformed for **1**·$CHCl_3$ and **1**·$^1/_2CH_2ClCH_2Cl$. Partial molecular orbital compositions in the ground state and absorption transition characters of **1**·$CHCl_3$ and **1**·$^1/_2CH_2ClCH_2Cl$ are summarized in Tables 6−9, respectively. The single electron density diagrams of the frontier molecular orbital involved in the absorption for **1**·$CHCl_3$ and **1**·$^1/_2CH_2ClCH_2Cl$ are depicted in Figures S15 and S16 (Supporting Information), respectively. The Pt-$(Me_3SiC{\equiv}CbpyC{\equiv}CSiMe_3)(C{\equiv}CPh)_2$ moiety in **1**·$CHCl_3$ or **1**·$^1/_2CH_2ClCH_2Cl$ is assumed as a discrete dimer. The absorption and emission of **1**·$CHCl_3$ and **1**·$^1/_2CH_2ClCH_2Cl$ with different crystal packing in stacking of planar platinum(II) moieties were thus calculated through TD-DFT. To confirm whether the Pt−Pt interactions exist in **1**·VOC with different solvate VOC, we investigated the Pt−Pt contacts in **1**·$CHCl_3$ and **1**·$^1/_2CH_2ClCH_2Cl$ using the Wiberg bond indices (WBIs)[43] with the Natural Bond Orbital (NBO 3.1) program.[44] The WBIs of Pt−Pt contact in **1**·$CHCl_3$ is 0.0184, much higher than that in **1**·$^1/_2CH_2ClCH_2Cl$ (0.0032). However, the WBIs of Pt−Pt contact in both structures is significantly less than that of ordinary Pt−N (0.2997 or 0.2964) and Pt−C (0.7002 or 0.7056) single bonds in **1**·$CHCl_3$, implying that the Pt−Pt contact is weak in **1**·$CHCl_3$. The WBIs are correlated with the Pt−Pt distances, in which the shorter the Pt−Pt distances, the higher the WBIs. The larger WBI in **1**·$CHCl_3$ (0.0184) results from the shorter Pt−Pt distance (3.3 Å). For **1**·$^1/_2CH_2ClCH_2Cl$, the much smaller WBI (0.0032) is due to quite long Pt−Pt distance (4.4 Å), implying the absence of effective Pt−Pt interaction.

As shown in Tables 6 and 7, the HOMO in **1**·$CHCl_3$ is primarily composed of 41.6% composition from Pt(5d) and 55.4% contribution from the π orbital of phenylacetylides. The compositions of HOMO-1, HOMO-2, HOMO-3, and HOMO-5 are similar to those of HOMO localized mainly on Pt(5d) and phenylacetylides. The LUMOs are mainly resident on $\pi^*(Me_3SiC{\equiv}CbpyC{\equiv}CSiMe_3)$ with a contribution of 94.4% for LUMO, 85.2% for LUMO+1, 84.8% for LUMO+3, and 90.8% for LUMO+4. On the one hand, the HOMO compositions from Pt(5d) orbitals are much higher for crystalline state **1**·$CHCl_3$ (41.6%) than those for **1** (26.0%) in dichloromethane solvent. On the other hand, the HOMO level is raised approximately 0.685 eV for **1**·$CHCl_3$ (−5.0023 eV) relative to that for **1** in dichloromethane (−5.6872 eV), thus inducing an obviously reduced HOMO−LUMO energy gap (Figure 5) for the dimeric platinum(II) species **1**·$CHCl_3$ (2.23 eV) than that for **1** in dichloromethane (2.90 eV). The Pt−Pt interaction between two adjacent planar platinum(II) moieties in **1**·$CHCl_3$ causes destabilization of the HOMO and reduces the HOMO−LUMO energy gap, and thus resulting in a significant red-shifted emission compared with that of **1**·$^1/_2CH_2ClCH_2Cl$ without Pt−Pt interaction. To obtain an intuitive understanding of this, the energy diagrams of frontier orbitals for **1** (in CH_2Cl_2 solvent) and crystalline state **1**·$CHCl_3$ and **1**·$^1/_2CH_2ClCH_2Cl$ are depicted in Figure 5. The calculated lowest singlet S1 composed of HOMO→LUMO (83%) and HOMO-2→LUMO (17%) can be thus assigned as ^{1}MMLCT (metal−metal-to-ligand charge-transfer) transition, mixed with some ^{1}LLCT character. The main TD-DFT calculated excitation energies for **1**·$CHCl_3$ tabulated in Table 7 are in good agreement with the experimentally measured absorptions for the solid-state **1**·$CHCl_3$ (Figure S13, Supporting Information). The lowest triplet excitations at 864 nm (HOMO→LUMO), 756 nm (HOMO-2→LUMO), and 748 nm (HOMO→LUMO+1 and HOMO-1→LUMO) calculated by TD-DFT are in reasonable agreement with the experimentally measured emission (λ_{em} = 780 nm), in which the emission origins can be assigned as an admixture of ^{3}MMLCT and ^{3}LLCT transitions in view of Pt−Pt interaction between adjacent planar platinum(II) moieties.[9b,45,46]

For crystalline state **1**·$^1/_2CH_2ClCH_2Cl$ (Table 6), the HOMO is primarily composed of the compositions from Pt(5d) (25.8%) and the π orbital of phenylacetylide (70.4%), comparable to the HOMO compositions of **1** (26% from Pt(5d) and 72% from phenylacetylide) in dichloromethane solvent (Table 3). The HOMO-1, HOMO-2, HOMO-4, and HOMO-5 are also localized on Pt(5d) and phenylacetylides (π). The LUMOs are mainly

(43) Breneman, C. M.; Wiberg, K. B. *J. Comput. Chem.* **1990**, *11*, 361.
(44) Glendening, E. D.; Badenhoop, J. K.; Reed, A. E.; Carpenter, J. E.; Weinhold, F. *NBO*, Version 3.1; 1995, Theoretical Chemistry Institute, University of Wisconsin: Madison.
(45) Koo, C. K.; Ho, Y. M.; Chow, C. F.; Lam, M. H. W.; Lau, T. C.; Wong, W. Y. *Inorg. Chem.* **2007**, *46*, 3603.
(46) Ma, B.; Li, J.; Djurovich, P. I.; Yousufuddin, M.; Bau, R.; Thompson, M. E. *J. Am. Chem. Soc.* **2005**, *127*, 28.

Table 5. Transitions of **1** in Dichloromethane, Calculated by the TD-DFT Method and the Polarized Continuum Model (PCM)

Tr.	transition	contribution	*E*, nm (eV)	o.s.	assignment	measured value (nm)
T1	HOMO→LUMO	74%	596 (2.08)	0.0000	^{3}LLCT/^{3}MLCT	616
T2	HOMO-1→LUMO	98%	538 (2.30)	0.0000	^{3}LLCT/^{3}MLCT	
S1	HOMO→LUMO	100%	556 (2.23)	0.0196	^{1}LLCT/^{1}MLCT	
S2	HOMO-1→LUMO	100%	497 (2.49)	0.1180	^{1}LLCT/^{1}MLCT	455
S7	HOMO-5→LUMO	76%	355 (3.49)	1.2482	^{1}MLCT	368
	HOMO→LUMO+1	20%			^{1}LLCT/^{1}MLCT	
S13	HOMO-1→LUMO+2	100%	310 (3.99)	0.3964	^{1}LLCT/^{1}MLCT	348
S21	HOMO→LUMO+4	100%	289 (4.29)	0.5152	^{1}IL	333
S31	HOMO-5→LUMO+2	28%	259 (4.80)	0.2999	^{1}IL	289
	HOMO→LUMO+5	53%			^{1}IL	

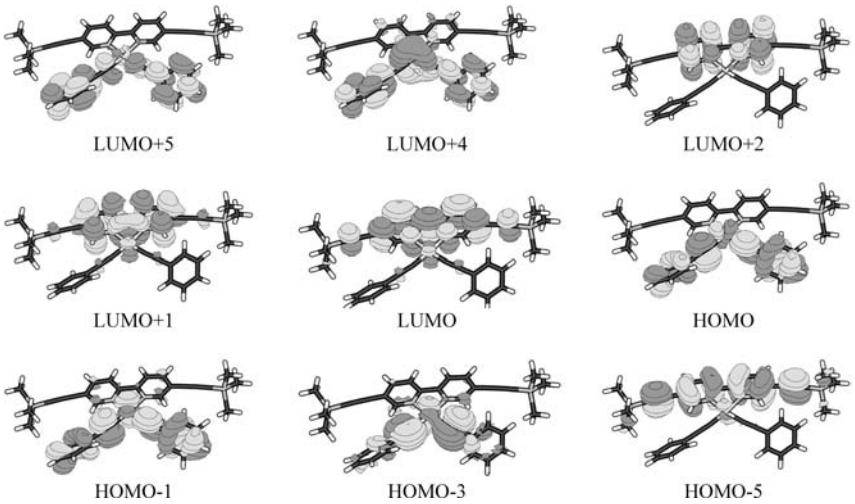

Figure 4. Electron-density diagrams of the frontier molecular orbitals involved in the absorption of **1** in dichloromethane solution.

Table 6. Partial Molecular Orbital Compositions (%) in the Ground State for Crystalline State **1**·$CHCl_3$ under the TD-DFT Calculations

		MO contribution (%)		
orbital	energy (eV)	Pt	$Me_3SiC{\equiv}CbpyC{\equiv}CSiMe_3$	C≡CPh
LUMO+4	−0.8381	5.0	90.8	4.2
LUMO+3	−1.2580	11.0	84.8	4.2
LUMO+2	−1.3399	16.8	78.0	5.2
LUMO+1	−2.5315	13.0	85.2	1.8
LUMO	−2.7750	3.6	94.4	2.0
HOMO	−5.0023	41.6	3.0	55.4
HOMO-1	−5.2888	28.4	5.0	66.6
HOMO-2	−5.3084	75.0	2.6	22.4
HOMO-5	−5.8132	51.6	7.4	41.0

Table 7. Transitions of Crystalline State **1**·$CHCl_3$, Calculated by the TD-DFT Method and the Polarized Continuum Model (PCM)

	transition	contribution	*E*, nm (eV)	o.s.
T1	HOMO→LUMO	88%	864 (1.43)	N/A
	HOMO-2→LUMO	12%		
T2	HOMO-2→LUMO	85%	756 (1.64)	N/A
T3	HOMO→LUMO+1	56%	748 (1.66)	N/A
	HOMO-1→LUMO	40%		
S1	HOMO→LUMO	83%	812 (1.53)	0.0070
	HOMO-2→LUMO	17%		
S3	HOMO→LUMO+1	83%	711 (1.74)	0.0079
	HOMO-2→LUMO+1	17%		
S11	HOMO-1→LUMO+2	96%	530 (2.34)	0.0409
S55	HOMO-5→LUMO+3	43%	326 (3.80)	0.3103
	HOMO-1→LUMO+4	20%		

contributed by π^* orbital of $Me_3SiC{\equiv}CbpyC{\equiv}CSiMe_3$. Because of the absence of Pt−Pt interaction in **1**·$^1/_2CH_2ClCH_2Cl$ as revealed from X-ray crystallography and WBI calculation, the calculated lowest singlet absorptions from HOMO-1→LUMO, HOMO→LUMO+1, and HOMO-

Table 8. Partial Molecular Orbital Compositions (%) in the Ground State for Crystalline State **1**·$^1/_2CH_2ClCH_2Cl$ under the TD-DFT Calculations

		MO contribution (%)		
orbital	energy (eV)	Pt	$Me_3SiC{\equiv}CbpyC{\equiv}CSiMe_3$	C≡CPh
LUMO+4	−1.0373	5.4	90.2	4.4
LUMO+1	−2.3530	4.0	93.6	2.4
LUMO	−2.4088	7.6	88.4	4.0
HOMO	−5.3449	25.8	3.8	70.4
HOMO-1	−5.3536	27.8	4.0	68.2
HOMO-2	−5.4564	25.6	5.4	69.0
HOMO-4	−5.8489	42.6	6.8	50.6
HOMO-5	−5.9046	43.0	6.6	50.4

Table 9. Transitions of Crystalline State **1**·$^1/_2CH_2ClCH_2Cl$, Calculated by the TD-DFT Method and the Polarized Continuum Model (PCM)

	transition	contribution	*E*, nm (eV)	o.s.
T1	HOMO-1→LUMO	73%	591 (2.10)	N/A
	HOMO-2→LUMO	9%		
T2	HOMO-1→LUMO+1	41%	584 (2.12)	N/A
	HOMO→LUMO	40%		
T3	HOMO→LUMO	48%	560 (2.21)	N/A
	HOMO-2→LUMO+1	24%		
	HOMO-1→LUMO+1	21%		
S1	HOMO-1→LUMO	97%	552 (2.25)	0.0240
S4	HOMO→LUMO+1	86%	537 (2.31)	0.0330
	HOMO-2→LUMO	9%		
S10	HOMO-5→LUMO	62%	454 (2.73)	0.1068
	HOMO-4→LUMO+1	34%		

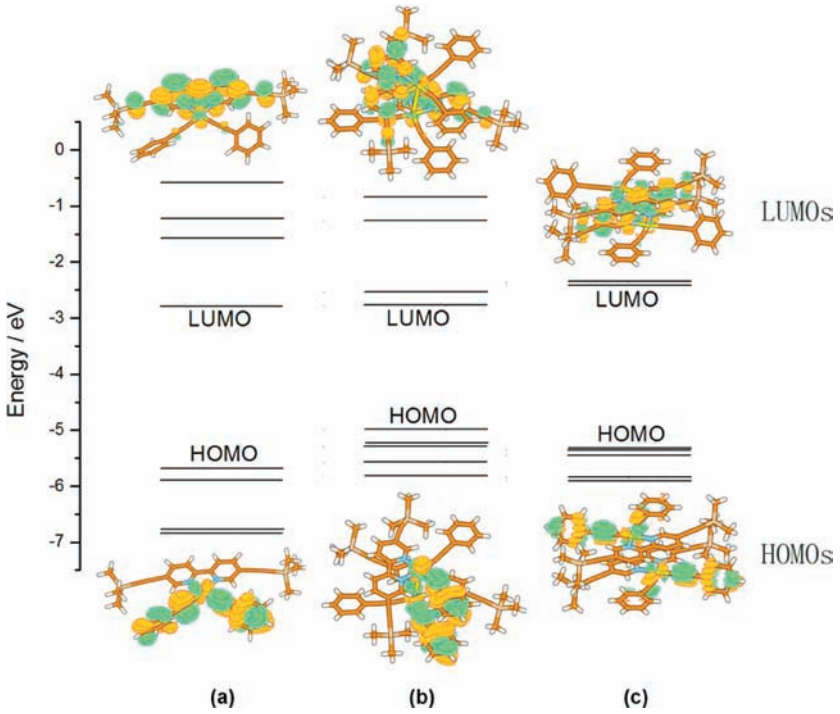

Figure 5. Diagrams of frontier orbital energy levels and electron-density of HOMO and LUMO by TD-DFT calculations. (a) **1** in CH_2Cl_2 solvent, (b) **1**·$CHCl_3$, and (c) **1**·$^1/_2(CH_2ClCH_2Cl)$.

5→LUMO (Table 9) transitions can be assigned as an admixture of ^{1}LLCT and ^{1}MLCT character. It is obvious that the HOMO−LUMO energy gap (2.84 eV) is also analogous to that of **1** in dichloromethane (2.90 eV), suggesting the behavior of planar platinum(II) moieties in crystalline state **1**·$^1/_2CH_2ClCH_2Cl$ is close to that of **1** in dichloromethane. The calculated absorption spectrum (black bars) coincides well with the measured UV−vis absorption spectrum of **1**·$^1/_2CH_2ClCH_2Cl$ (Figure S14, Supporting Information). The lowest calculated triplet excitations (591, 584, and 560 nm) are in good agreement with the experimentally measured emission (λ_{em} = 604 and 570 nm).

Vapochromic and Vapoluminescent Properties. Red solid sample **1** exhibits a bright orange emission at 561 (603sh) nm under UV (365 nm) irradiation. Upon exposure to a saturated vapor of dichloromethane, chloroform, or methyl iodide, the red sample **1** changed to dark brown in a few minutes. Meanwhile the bright red emission of **1** disappeared entirely and a weak structureless broadband centered at 761 nm was detected (Figure 6). In contrast, exposure of **1** to vapors of other volatile halohydrocarbon including carbon tetrachloride, 1,2-dichloroethane, 1,1,2-trichloroethane, dibromomethane, and tribromomethane did not induce any changes in the solid-state emission spectrum of **1**. Figure 6 depicts the emission spectra of solid-state **1** upon exposure to various halohydrocarbon vapors at ambient temperature, showing emission at approximately 770 nm for CH_2Cl_2, $CHCl_3$, and CH_3I vapors, and approximately 560 nm (610 nm) for other halohydrocarbon vapors such as carbon tetrachloride, 1,2-dichloroethane, 1,1,2-trichloroethane, dibromomethane, and tribromomethane. As revealed from TD-DFT calculation, the significant emission shift and dramatic color change of the red sample **1** upon exposure to the vapor of CH_2Cl_2, $CHCl_3$, or CH_3I arise most likely from a reversible conversion of emissive states from ^{3}MLCT/^{3}LLCT to ^{3}MMLCT/^{3}LLCT character.[3,8−13]

In most cases, the vapochromic properties of square-planar platinum(II) complexes with π-conjugated chelating ligands containing N^N, N^C, N^N^N, N^N^C, or N^C^N donors are highly sensitive to Pt···Pt distances that can be readily perturbed by the inserted solvate molecules in the crystal lattices. As found in the crystal structures of **1**·$CHCl_3$, Pt($Me_3SiC{\equiv}CbpyC{\equiv}CSiMe_3$)-($C{\equiv}Cbpy)_2$·VOC (HC≡Cbpy = 5-ethynyl-2,2′-bipyridine, VOC = $CHCl_3$ or THF),[31] and [Pt(TPPPB)Cl]Cl (TPPPB = 1-terpyridyl-2,3,4,5,6-pentaphenyl-benzene),[3a] a staggered packing with each planar platinum(II) moiety rotated in some extent along the stacking direction favors the formation of effective Pt−Pt contact. On the other hand, a face-to-face packing with direct overlapping is also in favor of forming Pt−Pt contact as well as $\pi\cdots\pi$ stacking.[3b,9,13] In contrast, a sliding antiparallel packing in stacking of the planar platinum(II) moieties is generally unfavorable for both Pt−Pt and $\pi\cdots\pi$ interactions.[3,31] Thus, the reversible luminescence vapochromism in platinum(II) complexes is essentially correlated with the interconversion between ^{3}MLCT and ^{3}MMLCT excited states. In contrast with the selective vapochromism of **1** to specific organic vapors including CH_2Cl_2, $CHCl_3$, and CH_3I, the complex Pt($Me_3SiC{\equiv}CbpyC{\equiv}CSiMe_3$)($C{\equiv}Cbpy)_2$ exhibits diverse extent of luminescence vapochromic properties to a variety of VOCs.[31] Interestingly, the emission of Pt($Me_3SiC{\equiv}CbpyC{\equiv}CSiMe_3$)($C{\equiv}Cbpy)_2$·VOC was progressively red-shifted in the order 562(610sh) (acetone)→617 nm (*n*-hexane)→660 nm (ethyl acetate)→729 nm ($CHCl_3$)→747 nm (THF). The emission energy is correlated well with the Pt···Pt

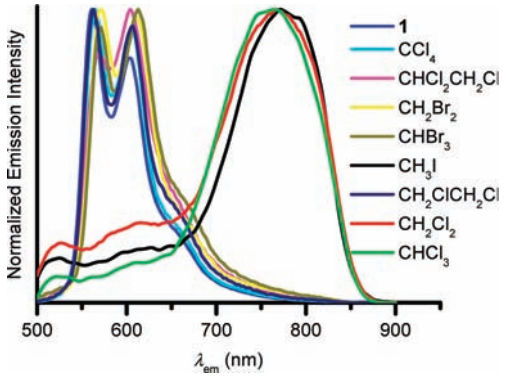

Figure 6. Emission spectra of solid-state **1** upon exposure to various halohydrocarbon vapors at ambient temperature, showing the emission at ca. 770 nm for CH_2Cl_2, $CHCl_3$, and CH_3I vapors, and ca. 560 nm (610 nm) for other halohydrocarbon vapors.

distances,[31] in which the shorter the Pt···Pt distance, the lower the emission energy of ^{3}MMLCT triplet state. The complex [Pt(TPPPB)Cl]Cl by Eisenberg et al.[3a] exhibited reversible and selective vapochromism to vapors of CH_2Cl_2, ethanol, ethyl acetate, and acetonitrile with 140 nm vapochromic shift, resulting from a disruption of the Pt−Pt interactions in the red form with a conversion of ^{3}MMLCT emitting state to a more-localized ^{3}MLCT excited state in the green form. Kato et al. reported the unusual luminescence vapochromic properties of a neutral platinum(II) complex [Pt(dcbpy)-$(CN)_2$] (dcbpy = 4,4′-dicarboxy-2,2′-bipyridine).[8b] This complex exhibited a stepwise luminescence vapochromism from 550 to 770 nm upon exposure to organic vapors with the sequence DMSO→DMF→CH_3CN→acetone→EtOH→AcOH→MeOH→benzene→$CHCl_3$, in which the emission energies are correlated with the dielectric constant of solvate VOCs.

In order to explore selectivity and reversibility of the vapochromic and vapoluminescent properties of **1** to specific VOCs, a THF solution of **1** was put on quartz disks that were purged with N_2 at ambient temperature. Upon exposure to vapors of various VOCs including ethyl ether, ethyl acetate, methyl acetate, acetone, methanol, ethanol, acetonitrile, pyridine, dibromomethane, carbon tetrachloride, 1,1,2-trichloroethane, toluene, 1, 2-dichloroethane, 1,2-dibromoethane, and bromoform, the deposited quartz disks display the same emission spectra (Figure S17, Supporting Information) as that recorded from the crystalline state **1** without solvate VOCs, which is red under ambient light and emits bright orange luminescence under UV light irradiation as shown in Figure S18 (Supporting Information). Upon exposure of the deposited quartz disks prepared in THF solution to a saturated vapor of dichloromethane, chloroform, or iodomethane, however, a rapid vapochromic response was observed, in which the deposited quartz disks turned dark brown from red in half a minute with a weak luminescence at 760 nm (Figure 6). On the other hand, if a dark brown quartz disk was exposed to a saturated vapor of THF or other VOCs except for dichloromethane, chloroform, or iodomethane, a rapid color change from dark brown to red was observed in half a minute and the bright orange luminescence was restored under UV irradiation. The vapochromic response is fully reversible and reproducible with no detectable degradation after several exposure cycles. It is convenient to exchange the solvent molecules by exposing one solvate complex to another organic vapor. Figure S18 (Supporting Information) shows photographic images of **1** deposited on quartz slices that were exposed to selected organic vapors under ambient light and UV light irradiation (365 nm). The color and luminescence of **1** show the distinct differences upon adsorbing CH_2Cl_2, $CHCl_3$, and CH_3I vapors in strikingly contrast to those of others. Undoubtedly, **1** exhibits a specific selectivity for detection volatile halohydrocarbon with one carbon atom and molecular weight less than 150.

Conclusions

Bis(σ-acetylide) platinum(II) complex **1** represents an example that displays unusual luminescence vapochromism to specific organic vapors and has potential application for detection of volatile halohydrocarbon with one carbon atom and molecular weight less than 150 in view of the highly reversible and selective vapochromism to CH_2Cl_2, $CHCl_3$, and CH_3I. Significant emission shifts and dramatic color changes of **1**·VOC with specific solvate VOCs have reasonably been interpreted by the crystal packing patterns and the Pt−Pt contact in stacking of the planar platinum(II) moieties. The solution and solid state absorption and emission properties were reasonably elucidated and well supported by DFT molecular orbital calculation. Both the experimental and TD-DFT calculation data suggest that the significant emission shift and dramatic color change upon exposure of solid-state **1** to the vapor of CH_2Cl_2, $CHCl_3$, or CH_3I result from a reversible conversion from ^{3}MLCT/^{3}LLCT to ^{3}MMLCT/^{3}LLCT emissive state.

Acknowledgment. We thank financial supports from the NSFC (20625101, 20773128, and 20821061), the 973 project (2007CB815304) from MSTC, the NSF of Fujian Province (2008I0027 and 2008F3117), and the major project from FJIRSM (SZD09001).

Supporting Information Available: Figures giving thermal analysis−mass spectra, additional UV−vis and emission spectra, tables and figures giving DFT calculation data, and X-ray crystallographic file in CIF format for the structure determination of compounds **1**, **1**·$CHCl_3$, **1**·$^1/_2$(CH_2ClCH_2Cl), and **1**·$^1/_2$(toluene). This material is available free of charge via the Internet at http://pubs.acs.org.